Applied Catalysis B: Environmental 97 (2010) 257–268

Contents lists available at ScienceDirect

Applied Catalysis B: Environmental

journal homepage: www.elsevier.com/locate/apcatb

SBA-15 type materials as support of catalysts based on ruthenium sulfide for sulfur removal

A. Romero-Pérez [a], A. Infantes-Molina [b], E. Rodríguez-Castellón [a], A. Jiménez-López [a,*]

[a] Departamento de Química Inorgánica, Cristalografía y Mineralogía (Unidad Asociada al ICP-CSIC), Facultad de Ciencias, Universidad de Málaga, Campus de Teatinos, 29071 Málaga, Spain
[b] Instituto de Catálisis y Petroleoquímica, CSIC, Cantoblanco, 28049 Madrid, Spain

ARTICLE INFO

Article history:
Received 26 January 2010
Received in revised form 8 April 2010
Accepted 10 April 2010
Available online 24 April 2010

Keywords:
Mesoporous SBA-15
Ruthenium sulphide
Dibenzothiophene
HDS

ABSTRACT

In the hydrodesulfuration (HDS) of dibenzothiophene (DBT) performed on catalysts derived from SBA-15-supported ruthenium sulfide systems, the roles of the support and the sulfiding temperature were studied. In this sense, three ruthenium sulfided catalysts supported on SBA-15 type materials have been prepared. The three employed supports were: a pure mesoporous silica SBA-15 (Si-SBA), that doped with zirconium (Zr-SBA) and that doped with aluminium (Al-SBA). The supports, precursor, sulfided and spent catalysts were characterized by X-ray diffraction (XRD), N_2 adsorption–desorption isotherms at −196 °C, NH_3-TPD, XPS analysis and H_2-TPRS. The catalytic properties of these materials in the hydrodesulfurization (HDS) of dibenzotiophene (DBT) were tested between 260 and 360 °C under a hydrogen pressure of 3.0 MPa. The catalytic activity increased when catalysts were sulfided at 500 °C because of the formation of a greater amount of RuS_2 having pyrite structure. Moreover, catalysts supported on Si-SBA and Zr-SBA turned out to be more active than that supported on Al-SBA due to a higher dispersion of the active phase, with conversions close to 100% at a reaction temperature of 360 °C.

1. Introduction

Environmental catalysis researchers worldwide have focused much attention on the development of catalytic systems capable of reducing the sulfur amount present in petroleum feedstocks until levels globally established by the recently enacted environmental protection laws. The issues of gasoline and diesel deep desulfurization are becoming more serious because the crude oils are getting higher in sulfur contents as long as the reduction of petroleum reserves provokes the usage of lower quality feedstocks, while the regulated sulfur limits are becoming lower and lower. In this regard, the maximum sulfur content present in the diesel fuel to obtain an Ultra Low Sulfur Diesel (ULSD) is of 10 ppm in the European Union from the beginning of 2009 with the entry into force of the Euro V fuel standard directive [1]. Meanwhile this limit is slightly higher in the United States, 15 ppm, regulated by the Environmental Protection Agency (EPA) [2]. Thus, the development of highly active and selective HDS catalysts, capable of processing these feeds, is one of the most important problems that the petroleum industry has to face nowadays.

Transition metal sulfides (TMS) have been traditionally used as active phases in hydrotreating catalysts since they are known to be efficient systems for catalyzing hydrotreating reactions. Concretely molybdenum or tungsten sulfides promoted by cobalt or nickel are the active phases and mainly porous γ-alumina is the material support of the catalysts for excellence in the hydrotreating industry. Amelioration has been achieved by modifying the properties of these sulphide systems, although the nature of the active phase has hardly been modified during many decades [3,4]. Moreover other transition metal sulfides such as chromium sulfide [5] have been tested in hydrodesulfurization of dibenzotiophene and the catalytic activity depended on the support employed. Kabe and co-workers [6] have studied the catalytic activity in the HDS of DBT of Cr, CrCu, CrNi and CrCo alumina supported catalysts and have found that the activity is directly correlated with the amount of labile sulfur in the surface, i.e., the weaker the chromium–sulfur bond the higher the number of labile sulfur atoms, leading so to an increase in the number of active sites. Contradictory results related to the performance of RuS_2 based catalysts have been published in the literature. The pioneering work of Pecoraro and Chianelli reported nonsupported ruthenium sulfide as the most active phase in hydrotreating reactions [7]. However, there is a large discrepancy when this phase is supported on different materials. Some authors found a low activity of this phase when supported because of both the incomplete sulfidation of ruthenium species and the instability of the RuS_2 phase on the support under hydrogen atmosphere. [8,9]. Notwithstanding, due to the promising HDS activity of the RuS_2 compound, attributable to its isotropic cubic structure where disul-

* Corresponding author. Tel.: +34 952131876; fax: +34 952137534.
E-mail address: ajimenezl@uma.es (A. Jiménez-López).

0926-3373/$ – see front matter © 2010 Elsevier B.V. All rights reserved.
doi:10.1016/j.apcatb.2010.04.010

fide species $(S–S)^{-2}$ seem to increase the surface density of the SH groups coming from the heterolytic dissociation of hydrogen [10], much effort has been devoted to prepare highly active RuS_2 supported catalysts for HDS reactions. A work of Quartararo et al. [11] pointed out that the activity of this compound is directly related to several parameters such as the reactant to treat, the employed support, the catalytic activation and testing conditions. In this sense, the catalyst activation has been considered of utmost importance in the HDS activity of ruthenium-supported catalysts. Bearing this in mind and from literature data, the calcination step of the precursor salt should be avoided, since it appears to reduce the initial high degree of dispersion for the impregnated and dried Ru catalyst [10–12]. The work of De los Reyes et al. [8] reported that the sulfidation in absence of hydrogen without prereduction or calcination allows the genesis of the pyrite phase along with the preparation of well dispersed and very active catalyst for thiophene hydrodesulfurization. The sulfidation process by a N_2/H_2S flow is reported to be more efficient than by a H_2/H_2S flow, providing more active ruthenium sulfided catalysts [13], because under a H_2 atmosphere it is known that sulfided Ru species can be reduced, decreasing so the HDS activity [11]. Moreover some authors have suggested that the sulfiding temperature affects not only the crystal size of RuS_2, but also could provide different crystallographic orientations, which can correlate with differences in catalytic activity [13]. The role of the support is another important issue to consider, relevant to industrial practice, in order to obtain more active and stable HDS catalysts. The support effect in the HDS reaction has been reviewed in detail [14,15]. Different materials have been tested as supports to study the role of support on the dispersion of the active phase as well as the influence of the metal–support interaction on the catalytic activity [14–16]. When Al_2O_3 is used as support of ruthenium sulfided catalysts, the addition of cesium favours the formation of more stable RuS_2 particles which do not undergo reduction into the Ru metallic form under the experimental hydrotreating conditions [17]. Eliche-Quesada et al. have found an excellent catalytic activity of ruthenium sulfide supported catalysts by using mesoporous silica MCM-41 doped with zirconium [18] as Zr ions stabilizes the RuS_2 active phase through an increase in the Ru–S bond strength. The potential advantage of mesoporous hosts for the preparation of catalytic phase materials lies in the high dispersion of the catalytic phase at high loadings. The use of SBA-15 as support for hydrotreating catalysts has presented several advantages with regard to HMS and MCM-41 mesoporous solids, i.e., SBA-15 material has thicker pore walls and better hydrothermal stability, which are very important for hydrotreating processes, which are carried out under severe reaction conditions. Several works have highlighted the advantages of SBA-15 in hydrotreating reactions [19,20].

Thus, in the present work we evaluate the properties of SBA-15 mesoporous silica as support of the RuS_2 phase in the HDS reaction of DBT and the presence of Al and Zr heteroatoms into the SBA-15 silica framework acting as stabilizer agents of the RuS_2-pyrite phase. For this purpose, three ruthenium sulfide catalysts supported on SBA-15 mesoporous silica (Si-SBA) and SBA-15 mesoporous silica doped with aluminium (Al-SBA) and zirconium (Zr-SBA) were tested in the hydrodesulfurization of dibenzothiophene. Moreover the role of the sulfidation temperature on the formation of the RuS_2 phase and the catalytic activity was as well studied.

2. Experimental

2.1. Materials

The supports used in this study were a SBA-15 mesoporous silica (Si-SBA) prepared using a low cost method [21], a SBA-15 mesoporous silica doped with zirconium with a Si/Zr molar ratio = 10 (Zr-SBA) prepared following the method described by Szczodrowski et al. [22], and a SBA-15 mesoporous silica doped with aluminium with a Si/Al molar ratio = 10 (Al-SBA) prepared as described by Gómez-Cazalilla et al. [23]. Ruthenium trichloride, $RuCl_3{\cdot}nH_2O$ (~41 wt% Ru, from Fluka) was employed as ruthenium precursor salt. The chemical products utilized in the reactivity study were dibenzothiophene (Aldrich 98%) in *cis*-, *trans*-decahydronaphthalene (Sigma–Aldrich 98%). The gases employed were H_2S/N_2 10/90% (Air Liquide 99.99%), He (Air Liquide 99.99%), H_2 (Air Liquide 99.999%), N_2 (Air Liquide 99.9999%) and NH_3 (Air Liquide 99.9%).

2.2. Preparation of catalysts

Three ruthenium sulfided catalysts supported on Si-SBA, Al-SBA and Zr-SBA were prepared.

Ruthenium was introduced by the incipient wetness impregnation method but using an aqueous solution of ruthenium(III) chloride ($RuCl_3{\cdot}nH_2O$). The concentration of the precursor solutions was adjusted to 7 wt% of ruthenium. Once the ruthenium aqueous solution was added to the pelletized support (0.85–1.00 mm), it was air-dried. Finally, the samples were sulfided *in situ* at atmospheric pressure with a N_2/H_2S (90/10%) flow of 60 ml min^{-1} by heating from rt. to the sulfidation temperature (T_s) (2 h) at a heating rate of 10 °C min^{-1}.

The catalyst precursors will be referred to as Ru*x*prec, being *x*: Si, Zr or Al if the support employed is Si-SBA, Zr-SBA and Al-SBA, respectively. The sulfided catalysts will be referred to as Ru*x*ST_s, being T_s the sulfidation temperature in °C.

2.3. Characterization of catalysts

X-ray diffraction patterns (XRD) of the precursor, sulfided and spent catalysts were obtained with a X′Pert PRO MPD Philips diffractometer (PANanalytical), using monochromatic CuKα radiation (λ = 1.5406 Å). The Kα radiation was selected with a Ge (1 1 1) primary monochromator. The X-ray tube was set at 45 kV and 40 mA.

The textural properties (S_{BET}, V_p, d_p) of the sulfided catalysts were obtained from the N_2 adsorption–desorption isotherms at −196 °C measured with a Micromeritics ASAP 2020 apparatus. Prior to the measurements, the samples were outgassed at 200 °C and 10^{-4} mbar overnight. Surface areas were determined by using the Brunauer–Emmet–Teller equation [24] and a nitrogen molecule cross-section of 16.2 $Å^2$. The pore size distribution was calculated by applying the Barrer–Joyner–Halenda method (BJH) to the desorption branch of the N_2 isotherm. The total pore volume was calculated from the adsorption isotherm at $P/P_0 = 0.98$.

Transmission electron micrographs of the precursor, sulfided and spent catalysts were obtained by using a Philips CM 200 Supertwin-DX4 microscope. Samples were dispersed in ethanol. A drop of the suspension was put on a Cu grid (300 mesh).

Temperature-programmed desorption of ammonia (NH_3-TPD) was carried out to evaluate the total acidity of the catalysts. Catalysts were sulfided at atmospheric pressure by flowing the sulfiding mixture from room temperature to the sulfidation temperature with a heating rate of 10 °C min^{-1} and maintaining the sample at this temperature for 2 h. After cleaning with helium and adsorption of ammonia at 100 °C, the NH_3-TPD was performed between 100 and 600 °C with a heating rate of 10 °C min^{-1} by using a helium flow. The evolved ammonia was analyzed by on-line gas chromatography (Shimadzu GC-14A) provided with a TCD.

Hydrogen temperature-programmed reduction (H_2-TPRS) of the sulfided catalysts were carried out between 50 and 800 °C using a flow of 10% H_2/Ar (48 ml min^{-1}) and a heating rate of 10 °C min^{-1}.

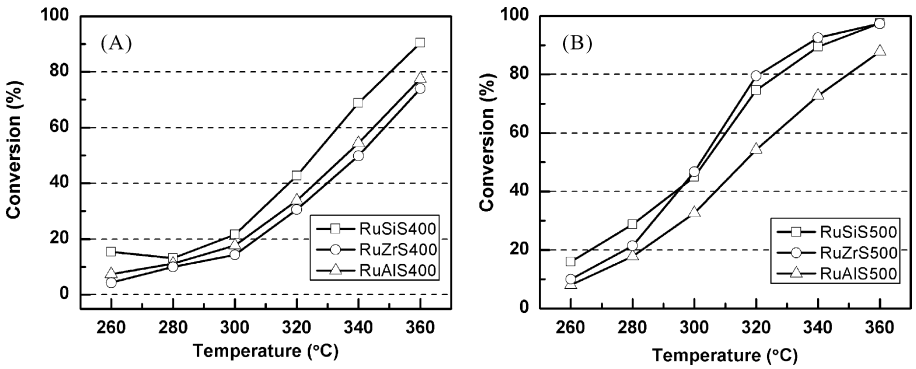

Fig. 1. Total DBT conversions as a function of reaction temperature for: (A) Ru*x*S400 catalysts and (B) Ru*x*S500 catalysts. Reaction conditions: P = 30 bar, WHSV = 32 h^{-1}, and H_2 = 100 ml min^{-1}.

Prior to the analysis the precursors were sulfided *in situ* at 400 °C or 500 °C (2 h) using a flow of H_2S/N_2 (10/90% with a flow rate of 60 ml min^{-1}). After that, a helium flow (60 ml min^{-1}) was passed for 30 min at 50 °C to clean the sample. Water produced in the reduction reaction was removed by passing the gas flow through a cold finger (−80 °C). The H_2-TPRS experiments were registered by using an on-line quadrupole mass spectrometer Balzer GSB 300 02.

Elemental chemical analysis of carbon, nitrogen, hydrogen and sulfur for (CHNS) spent catalysts was performed with a LECO CHNS 932 analyzer.

X-ray photoelectron spectra were collected using a Physical Electronics PHI 5700 spectrometer with non-monochromatic Al K_α radiation (300 W, 15 kV, and 1486.6 eV) with a multi-channel detector. Spectra of pelletized samples were recorded in the constant pass energy mode at 29.35 eV, using a 720 μm diameter analysis area. Charge referencing was measured against adventitious carbon (C 1*s* at 284.8 eV). A PHI ACCESS ESCA-V6.0 F software package was used for acquisition and data analysis. A Shirley-type background was subtracted from the signals. Recorded spectra were always fitted using Gaussian–Lorentzian curves in order to determine the binding energy of the different element core levels more accurately. Sulfided and spent catalysts were stored in sealed vials with an inert solvent. The sample preparation was done in a dry box under a N_2 flow, where the solvent was evaporated prior to its introduction into the analysis chamber, and directly analyzed without previous treatment.

2.4. Catalytic activity

As catalytic test, the hydrodesulfurization of DBT was chosen, which was performed in a high-pressure fixed-bed continuous-flow stainless steel catalytic reactor (9.1 mm in diameter, and 230 mm in length), operated in the down-flow mode. The reaction temperature was measured with an interior placed thermocouple in direct contact with the catalyst bed. The organic feed consisted of a solution of DBT (1 wt%) in decalin that was supplied by means of a Gilson 307SC piston pump (model 10SC). For the activity tests, 0.5 g of catalyst was used (particle size 0.85–1.00 mm) and was diluted with quartz sand to 3 cm^3. Prior to the activity test, the catalysts were sulfided *in situ* at atmospheric pressure with a N_2/H_2S (90/10%) flow of 60 ml min^{-1} by heating from rt. to 400 °C or 500 °C (2 h) at a heating rate of 10 °C min^{-1}. Catalytic activities were measured at different temperatures (260–360 °C) with a heating rate of 5 °C min^{-1}, under 3.0 MPa of H_2, with a H_2 flow rate of 100 ml min^{-1}, with an organic feed of 0.3 ml min^{-1} and with a hourly space velocity (WHSV) of 32 h^{-1}. The evolution of the reaction was monitored by collecting liquid samples after 60 min at the desired reaction temperature. Moreover, the stabilities of the catalysts were studied at a constant temperature reaction for 9 h, collecting samples after each hour of reaction. These samples were kept in sealed vials and subsequently analyzed by gas chromatography (Shimadzu GC-14B, equipped with a flame ionization detector and a capillary column, TBR-14, coupled to an automatic Shimadzu AOC-20i injector). For these catalysts, the main reaction products were biphenyl (BP), cyclohexylbenzene (CHB), bicyclohexyl (BCH), benzene (B) and cyclohexane (CH). For this reason, the total conversion was calculated from the ratio of converted dibenzothiophene/initial dibenzothiophene. The selectivity of the different reaction products was calculated considering BP, CHB, B and CH as the only products obtained, since only slight traces of some unknown compounds were noticeable in a few cases.

3. Results and discussion

3.1. Catalytic study

Ruthenium sulfide based catalysts supported on SBA-15 type materials were sulfided at 400 °C and 500 °C and their catalytic properties were tested on the HDS of dibenzothiophene. The activity studies were performed between 260 and 360 °C. Fig. 1 depicts the conversion data for the present series of catalysts where both the influence of the sulfiding temperature and the employed support are observed. There is a direct improvement in the conversion as a function of the reaction temperature. By focusing on the influence of the sulfiding temperature it is seen how the catalysts sulfided at 400 °C are less active. At this temperature, the catalyst supported on Si-SBA present the highest conversion values at all studied temperatures. Regarding catalysts supported on Si-SBA and Zr-SBA sulfided at 500 °C, they both convert more DBT molecules at all studied temperatures than their counterparts sulfided at 400 °C, being this increment in the conversion much more important for RuZrS500 catalyst. On the other hand, RuAlS500 catalyst turns out to be less active at both sulfiding temperatures.

By considering the selectivity data, all the catalysts preferentially undergo through the DDS route, i.e., the formation of byphenyl is favoured in all cases (Fig. 2). The influence of the sulfiding temperature reveals that by increasing it from 400 to 500 °C, the formation of the product coming from the HYD route, cyclohexylbenzene (CHB) increases slightly even at higher temperatures of reaction (Fig. 2) for RuSiS500 and RuZrS500, what should be related to the formation of more active phase. Taking into account the influence of the material support, catalysts supported on Al-SBA, present the lowest selectivity values toward CHB, and are the unique catalyst that present traces of benzene.

The increment in HDS activity with the reaction temperature can be explained by the formation of coordinatively unsaturated sites (CUS) during the test, as long as, the reducing conditions employed favour the removal of the excess and superficial sulfur atoms [25].

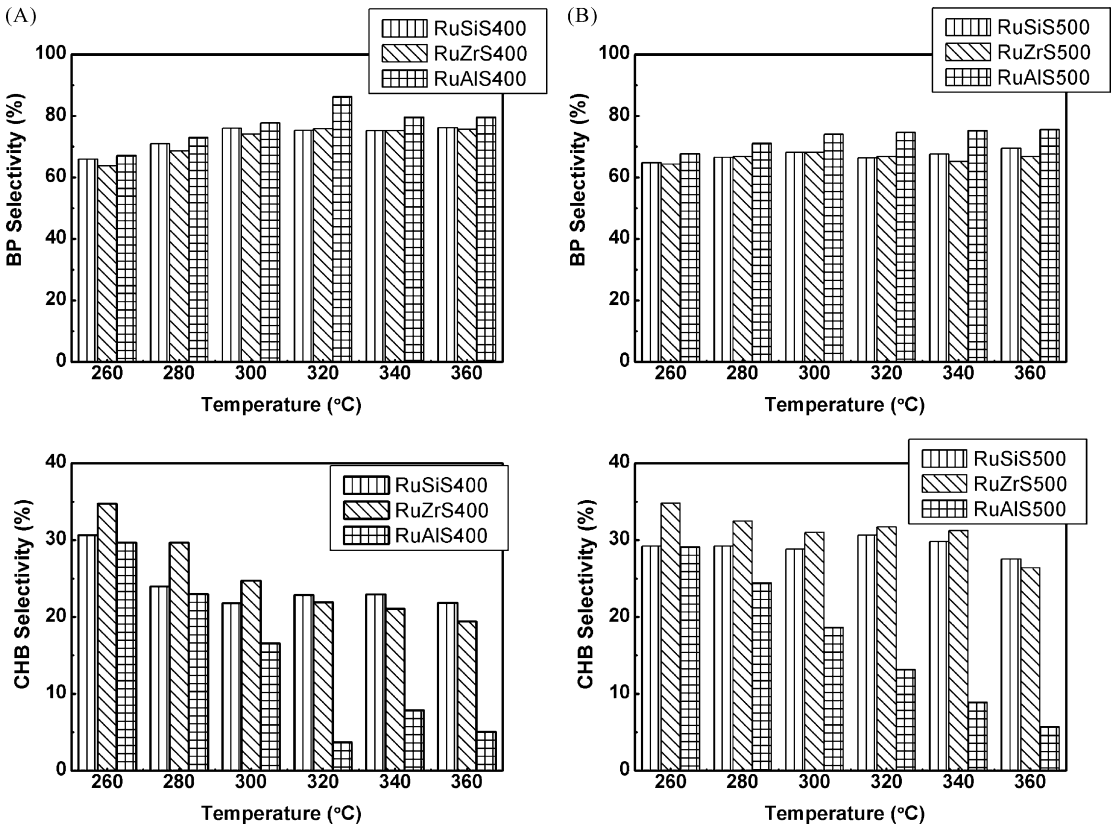

Fig. 2. Selectivities of DDS and HYD product for (A) RuxS400 catalysts and (B) RuxS500 catalysts. Reaction conditions: $P = 30$ bar, WHSV = 32 h^{-1}, and H_2 = 100 ml min^{-1}.

These (CUS) are considered of uppermost importance in the HDS activity of transition metal sulphides (TMS) [26]. Nonetheless, thermodynamic aspects should also be considered here. In this regard and focusing on the selectivity data (Fig. 2), it is BP the product favoured at all studied temperatures. The formation of this product comes from the Direct Desulfurization (DDS) route of DBT which is favoured at higher temperatures as endothermic reaction. In contrast, the formation of CBH is exothermal and has to decrease with the increment of temperature; however, the catalyst sulfided at 500 °C maintains constant values of CHB product until 340 °C. It could indicate than more hydrogenation sites are generating during the reaction.

The rate constants for these catalysts were also calculated and compiled in Table 1. From these data, it can be seen that the rate constants increase with the sulfiding temperature, i.e., at 500 °C of sulfiding temperature the rate constants are higher. These data are in agreement with our previous statement, the formation of more RuS_2 with a pyrite-like structure at this temperature is the responsible of such behaviour. Moreover, it has been also calculated the activation energies by an Arrhenius type plot (Fig. 3), $lnk = f(1/T)$, and the data (Table 1) are in line with others reported in the literature [17]. Fig. 3 shows the Arrhenius type plot for RuSiS500 catalyst, considered as representative. In all cases, a single straight line is always observed and the found values of E*a* (Table 1) reveal that the HDS reaction is on the kinetic control regime.

In order to study the catalytic stability, the most active catalysts, RuSiS500 and RuZrS500, were working at 360 °C for nine hours. The corresponding results are plotted in Fig. 4, where both, conversion and selectivity data are lumped together. It can be observed how after 9 h, RuZrS500 and RuSiS500 catalysts maintain their catalytic activity with a conversion value close to 100% and a selectivity to BP of 67.5% and 74.5%, respectively, while RuAlS500 catalyst begins with a conversion value of 95% and after 9 h of reaction the conversion value decreased slightly up to 92%, observing a trend of the loss of its catalytic activity.

In order to gain further insight of the performance of these systems, a fully characterization of sulfided and spent catalysts have been carried out by several experimental techniques.

Table 1
Rate constants and activation energies of catalysts sulfided at 400 °C and 500 °C in the HDS of DBT reaction.

Temperature (°C)							
Catalyst	260	280	300	320	340	360	E_a (kJ mol^{-1})
$k \times 10^5$ (mol $gcat^{-1}$ min^{-1})							
RuSiS400	0.49	0.41	0.71	1.63	3.41	6.83	104.2
RuSiS500	0.51	0.99	1.74	4.00	6.58	10.84	87.6
RuAlS400	0.23	0.35	0.57	1.21	2.29	4.36	84.6
RuAlS500	0.25	0.58	1.15	2.28	3.80	6.15	90.3
RuZrS400	0.13	0.31	0.45	1.07	2.02	3.94	94.2
RuZrS500	0.31	0.70	1.84	4.63	7.59	10.62	103.9

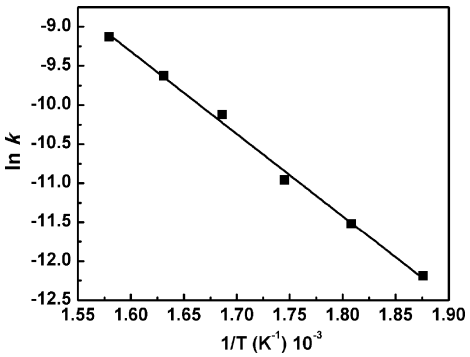

Fig. 3. Arrhenius plot for RuSiS500 catalyst.

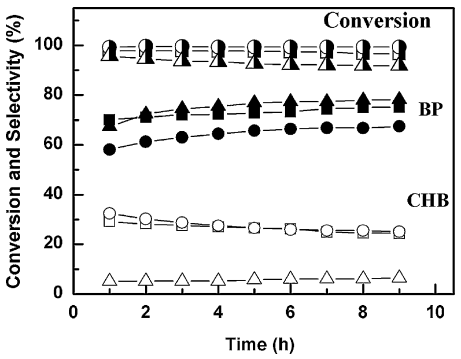

Fig. 4. Stability with time on stream for: (■) RuSiS500, (●) RuZrS500 and (▲) RuAlS500.

3.2. Catalyst characterization

3.2.1. XRD

The formation of crystalline phases was verified by X-ray powder diffraction of the precursor and the sulfided catalysts. As catalyst precursors as sulfided catalysts presented a reflection line at $2\theta \approx 1.2^\circ$ due to the d_{100} reflection of the mesoporous structure and reveals that the SBA framework has been maintained after the impregnation and sulfidation processes. On the other hand, the X-ray diffractograms at high angles of catalyst precursors did not show reflection lines due to the amorphous nature of hydrated ruthenium chlorides and/or oxychlorides [27,28]. However, after the sulfidation process (Fig. 5), new reflection lines at $2\theta = 31.8^\circ$, 45.7° and 54.2° appear and correspond to the [2 0 0], [2 2 0] and [3 1 1] diffraction signals of the RuS_2-pyrite phase (PDF Card No. 00-012-0737). If the diffractograms of the catalysts sulfided at 400 °C and 500 °C are compared, at 400 °C of sulfiding temperature, only the main diffraction line of the RuS_2 compound at $2\theta = 31.8^\circ$ is slightly noticeable (Fig. 5A), meanwhile when it is sulfided at 500 °C (Fig. 5B), the diffraction lines of the pyrite phase become more intense and well defined, indicating a greater formation of the RuS_2 phase which is also more crystalline, being especially intense for RuAlS500.

XRD measurements were also performed for spent catalysts. The corresponding diffractograms for catalysts sulfided at 500 °C (Fig. 5D) present the diffraction signals of the RuS_2-pyrite phase what indicates the high stability of the ruthenium sulfide particles formed after sulfidation at 500 °C. Meanwhile, the catalysts sulfided at 400 °C (Fig. 5C) suffer a slight loss of such crystalline domains. Moreover, they present the appearance of a new and broad peak at $2\theta = 43^\circ$ corresponding to the [1 0 1] plane of the metallic phase (Fig. 5C), indicating that the system becomes biphasic. The peaks

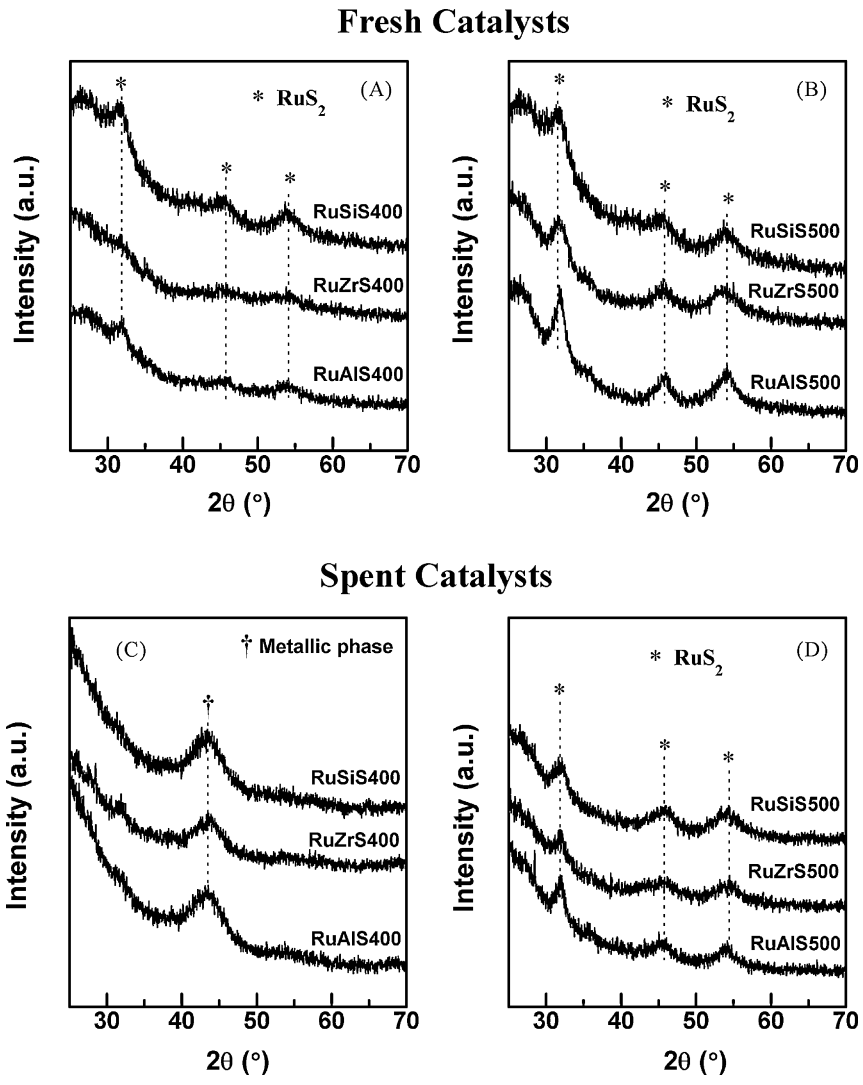

Fig. 5. Powder X-ray diffraction patters for: (A) RuxS400; (B) RuxS500, (C) RuxS500 spent catalysts and (D) RuxS400 spent catalysts.

Table 2
Textural properties of the samples.

Sample	S_{BET} ($m^2\ g^{-1}$)	V_p ($cm^3\ g^{-1}$)[a]	d_p (nm)[b]
Support			
Si-SBA	476	0.35	3.9
Zr-SBA	495	0.40	3.7
Al-SBA	360	0.29	3.7
Sulfided catalysts			
RuSiS400	331	0.25	3.5
RuZrS400	327	0.26	3.7
RuAlS400	222	0.18	3.2

[a] V_p at 0.98 P/P_0.
[b] Calculated by BJH method.

corresponding to RuS_2 are hardly visible. The lower formation of stable RuS_2-pyrite phase at this temperature, provokes that the amorphous or poorly crystallize ruthenium sulfide phase undergoes reduction under hydrogen hydrotreating atmosphere [29]. In this sense, other authors also pointed to an extend of reduction of 100% for silica supported ruthenium sulfide catalysts under an hydrogen atmosphere at a temperature of 400 °C [30]. Therefore a sulfidation temperature of 400 °C seems to be insufficient to form stable RuS_2 particles, i.e., possibly particles with a stoichiometry of RuS_{2-x} must be formed. Contrary to this are the spent catalysts sulfided at 500 °C which do not present the diffraction signals of metallic ruthenium. Therefore, at 500 °C, a greater proportion of pyrite phase is formed, which is highly stable under reaction conditions. In general it can be pointed to a high stability of the pyrite particles prepared on SBA-15 type materials, mainly sulfided at 500 °C.

3.2.2. Nitrogen adsorption–desorption isotherms at 77 K

The textural properties of the support, catalyst precursors and sulfided catalysts were evaluated by N_2 adsorption–desorption isotherms at −196 °C and the corresponding data are compiled in Table 2. Firstly, it should be noted that the isotherms of type-IV according to IUPAQ classification and typical of mesoporous materials are observed after impregnation and sulfidation processes, corroborating the stability of the framework. The surface area, calculated by the BET method, and pore volume suffer a decrease after the incorporation of the ruthenium (III) chloride salt and sulfidation. The observed decrease is explained by a partial pore blocking due to the incorporation of ruthenium into the channels of the support as will be clearly seen by TEM micrographs (Figs. 6 and 7). This fact occurs in a greater extend with the Al-SBA support, where the reduction of the surface area is a 38%.

3.2.3. TEM

TEM analysis of precursor, sulfided and spent catalysts was undertaken to estimate the distribution of the active phase.

Micrographs corresponding to sulfided catalysts (Fig. 6A–F) present different distribution of the active phase depending on the support employed, although in general no large ruthenium sulfided particles have been formed. The sulfided catalysts supported on Si-SBA and Zr-SBA show spherical particles with very small size, homogenously dispersed, strongly interacting with the support and mainly located inside the structure. This distribution is observed at both sulfiding temperatures, 400 and 500 °C. The location of the ruthenium sulfide particles inside the pores of the mesoporous structure is clearly observed in the micrograph corresponding to RuSiS500 sample (Fig. 6B), where an alignment of the RuS_2 phase is observed. The distance between two rows corresponds to the d_{100} parameter of the mesoporous structure. By measuring the distance between two rows, we obtain a value of 9.5 nm. If we compare this data with that calculated from the XRD pattern of the support at low angles, that presents the d_{100} reflection at $2\theta = 1.12°$, we obtained an a_0 value of 9.1 nm. Therefore we can assess that ruthenium sulfide particles are homogeneously located inside the pores.

On the other hand, the sulfided catalysts prepared from Al-SBA material support (Fig. 6E and F), present a different distribution of the active phase. We find small ruthenium sulfide particles inside the channels and larger particles located at the external surface of the support and scarcely interacting with this. A larger particle size is also found for these samples from XRD analysis.

The study of spent catalysts by TEM (Fig. 7) reveals the high stability of the RuS_2 particles during the catalytic test, as can be seen in Fig. 7A and B corresponding to RuSiS400 and RuZrS400 samples, respectively. These two catalysts present a homogenous distribution of small particles inside the channels with a size lower than 10 nm. No one suffers an increment in the particle size when increasing the sulfiding temperature 100 °C. Fig. 7C shows the micrograph of the RuAlS400 spent catalyst. It can be clearly observed the different distribution of the active phase on this support. Although we find zones where small and dispersed particles are found, the general tendency is the appearance of zones where agglomerates are present.

Taking into account the above results, it can be summarized that a better dispersion of the active phase is achieved when Si-SBA and Zr-SBA are used as support.

From TEM analysis it can be seen that the small-sized particles are inside the pores of the carriers. Nonetheless the pores are not blocked by the incorporation of ruthenium, as long as, N_2 adsorption–desorption isotherms of sulfided catalysts are similar to the material support (type-IV) and only a slight decrease in the surface area is observed as a consequence of the location of RuS_2 particles inside the channels.

3.2.4. NH_3-TPD

The acidic properties of this family of catalysts are determined by the amount of NH_3 reversibly adsorbed at 100 °C. The integration of the ammonia desorption curves allow us to know the amount of acid sites and the desorption temperature reveals us their strength. Fig. 8 compiles the NH_3-TPD profiles of pristine Zr-SBA and the RuZrS400 catalyst, as representative.

The integration data of the NH_3-TPD curves at different intervals of temperature for the bare supports, and sulfided catalysts are summarized in Table 3. The acidity of the supports follows the order Zr-SBA ≫ Al-SBA > Si-SBA, i.e., the incorporation of the heteroatom into the silica framework increases the acidity of the mesoporous material. The data presented in Table 3 show that the incorporation of zirconium (Zr-SBA) has led to a mesoporous material with a higher and stronger acidity than the incorporation of aluminium (Al-SBA) that only provides a material slightly more acid than the mesoporous silica (Si-SBA). Although all the supports desorb the majority of ammonia molecules at temperatures lower than 300 °C, pointing to acid centers of medium strength, Zr-SBA support also desorbs a 24% of the ammonia molecules at temperatures higher than 300 °C what reveals the existence of acid centers with a higher strength on this material.

After sulfiding, the acidity of the RuZrS400 sample slightly decreased with regard to the bare support as can be seen in Table 3. However, the acidity of RuSiS400 and RuAlS400 samples increased. It has been reported that the acidity of ruthenium sulfided catalysts is due to the presence of different species on the surface: coordinatively unsaturated sites (CUS) that provide Lewis acidity as well as SH groups providing Brönsted acidity [29].

3.2.5. XPS

As long as the catalytic performance of these systems is attributable to the formation of ruthenium sulfide, XPS spectra were recorded for precursor, sulfided and spent catalysts in order

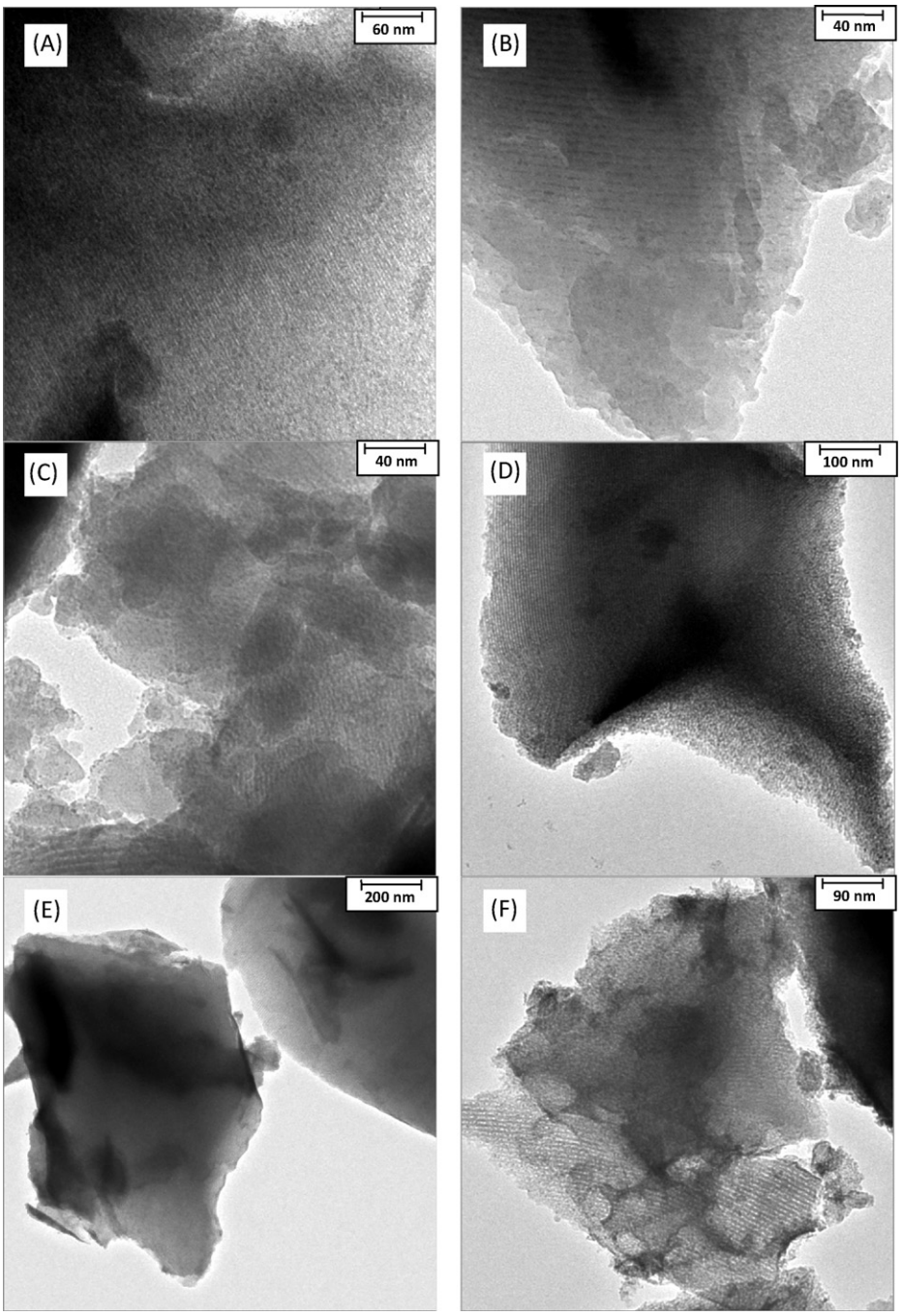

Fig. 6. TEM micrographs for: (A) RuSiS400; (B) RuSiS500; (C) RuZrS400; (D) RuZrS500; (E) RuAlS400; (F) RuAlS500.

to elucidate the chemical state of the elements present. The Al 2*p*, O 1*s*, Si *2p*, and Zr 3*d* core-level spectra were similar for precursor, sulfided and spent catalysts as well as their binding energies values maintained practically constant.

Ruthenium species were analyzed by recording the Ru 3*p* spectrum of the samples and studied by an appropriate curve fitting. Fig. 9 depicts the Ru 3*p* core-level spectra of RuSiS500 sample, as representative, while Table 4 lumps together the Ru $3p_{3/2}$ and S $2p_{3/2}$ binding energy values for all the samples, along with the S/Ru and Ru/X (X = Si+ (Si + Zr) or (Si + Al)) atomic ratios. Fig. 9A depicts the Ru $3p_{3/2}$ signals for RuSiPrec sample. The signal is slightly asymmetric and can be decomposed into two contributions: one centered at ca. 462.6-463-2 eV, that can be assigned to the presence of Ru species in the $RuCl_3$ compound, and a small one at ca. 465.5 eV, which is assigned to the presence of RuO_xCl_y containing Ru(IV) as a result of air oxidation of the precursor salt at room temperature during the preparation of the sample [31]. Our starting ruthenium salt, the commercially hydrated ruthenium trichloride, is actually a mixture of different ruthenium compounds with oxidation states of +III or +IV [32,33].

After the sulfidation process (Fig. 9B), the Ru $3p_{3/2}$ signal slightly shifts to lower BE although it remains asymmetric. For all sulfided catalysts, this signal is also decomposed into two contributions: the main one with its maximum between 460.8 and 461.4 eV; and a second one, much less intense whose maximum is between 463.2 and 463.8 eV. The main signal can be assigned to RuS_2 phase [34]. Mitchell et al. [35] reported, for ruthenium sulfide supported on alumina, Ru $3p_{3/2}$ binding energy values of 461.1-461-2 eV. While

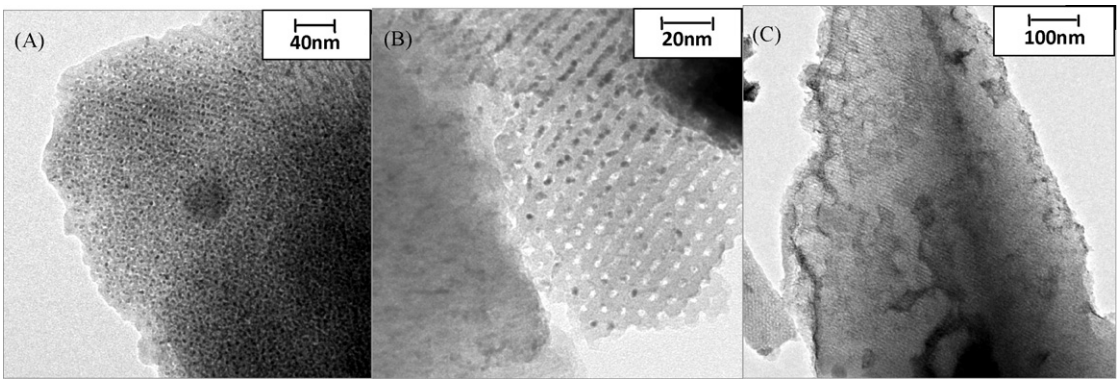

Fig. 7. TEM micrographs for: (A) RuSiS500, (B) RuZrS500 and (C) RuAlS500 spent catalysts.

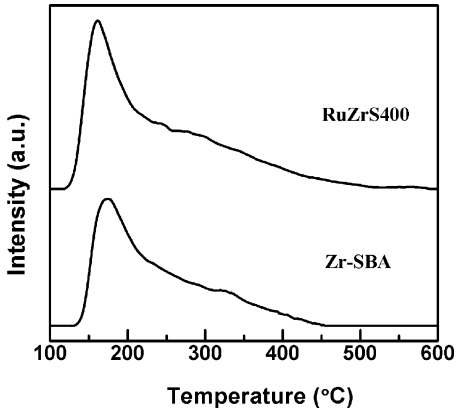

Fig. 8. NH_3-TPD profiles for Zr-SBA support and catalyst sulfided at 400 °C.

the weak peak (463.2–463.8 eV) should be due to Ru^{n+} species. Although some authors have assigned it to $RuCl_3$ species [18,34], no Cl 2*p* signal is observed after the sulfidation procedure, therefore it should be discarded this compound as responsible of such a peak.

With regard to the intensity of the Ru $3p_{3/2}$ signal, it should be noted that the Ru 3*p* band does not increase when increasing the sulfidation temperature, in no case. However, it is much more defined for catalysts prepared from Al-SBA as support. These results agree well with data obtained from XRD and TEM analyses, where a lower dispersion is found for this catalyst. Moreover, catalysts supported on Si-SBA and Zr-SBA present the majority of the active phase highly dispersed and mainly located inside the pores and the metallic particles, inside the porous structure with a wall thickness of ca. 50 Å, are not detected by XPS due to the surface sensitivity nature of this technique [36].

The S 2*p* core-level signals are always asymmetric and can be decomposed in two peaks ascribed to the doublet S $2p_{3/2}$ and S $2p_{1/2}$. The S $2p_{3/2}$ peak for sulfided catalysts is localized at BE ranged between 162.0 and 162.4 eV. This binding energy value is akin to that reported for sulfur forming disulfide polyanions $(S–S)^{2-}$ [8], i.e., sulfur forming RuS_2 with pyrite structure. This peak is present in all the samples and at both sulfided temperatures. In no case a peak centered at a BE value of ca. 161.5 eV is observed and assigned in the literature to S^{2-} ions [8]. It should be noted that both catalysts supported on Si-SBA (RuSiS400 and RuSiS500) possess along with the S $2p_{3/2}$ ascribed to S_2^{2-} ions another contribution at higher binding energies, 168.8 eV, due to the presence of sulfate species [34], as a consequence of a partial oxidation of the catalysts and also found by other authors [8].

As far as spent catalysts are concerned, the Ru $3p_{3/2}$ signal is hardly modified (Table 4), only a slight increase in the intensity of such a band is observed for catalysts supported on Zr-SBA and Al-SBA. Contrary is the S 2*p* signal, which suffers a slight shift to lower binding energies and in some cases it is not detected. As reported for many authors [29,30], during the catalytic run, due to the reducing atmosphere, sulfur can be eliminated from the catalyst surface and that is why a modification of the S 2*p* signal is observed. In fact, from XRD analysis of spent catalysts, those sulfided at 400 °C showed the presence of metallic ruthenium, confirming this fact. Moreover, Navarro et al. [37] reported that a large amount of sulfur vacancies

Table 3
Quantity of ammonia desorbed at different intervals of temperature.

Sample	μmol NH_3 g^{-1}					
	Temperature (°C)					
	100–200	200–300	300–400	400–500	500–600	Total
Si-SBA	131.2	12.7	–	–	–	143.9
Zr-SBA	457.9	359.8	197.1	57.1	8.8	1080.7
Al-SBA	113.8	50.4	17.4	10.5	–	192.1
RuSiS400	178.4	89.4	4.5	–	–	272.3
RuZrS400	318.7	317.6	144.4	16.9	–	797.6
RuAlS400	222.1	129.3	74.3	40.6	2.2	468.5

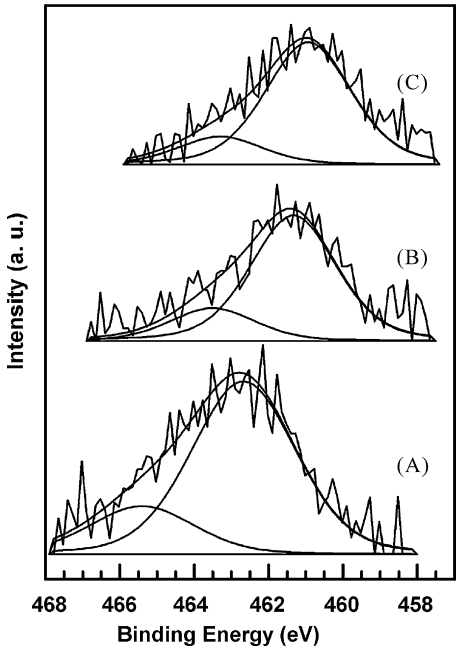

Fig. 9. Ru 3*p* core-level spectra for RuSiS500: (A) catalyst precursor; (B) sulfided catalyst; (C) spent catalyst.

Table 4
Spectral parameters and surface atomic ratios of precursors, sulfided and spent catalysts obtained by XPS analysis.

Sample	Binding energy (eV)					S/Ru[b]	Ru/X[a,b]
	Ru 3p$_{3/2}$				S 2*p*$_{3/2}$		
	$RuCl_3$	RuO_xCl_y	RuS_2	Ru^{n+}			
Catalysts precursors							
RuSiPrec	462.6	465.4	–	–	–	–	0.007
RuZrPrec	462.8	465.4	–	–	–	–	0.011
RuAlPrec	463.2	465.5	–	–	–	–	0.081
Sulfided catalysts							
RuSiS400	–	–	461.4	463.2	162.4	6.2	0.006
RuSiS500	–	–	461.3	463.5	162.4	7.0	0.004
RuZrS400	–	–	461.4	463.2	162.3	2.4	0.012
RuZrS500	–	–	461.1	463.8	162.3	2.3	0.010
RuAlS400	–	–	461.0	463.2	162.0	3.5	0.093
RuAlS500	–	–	460.8	463.2	162.0	3.4	0.076
Spent catalysts							
RuSiS400	–	–	461.1	463.3	–	–	0.010
RuSiS500	–	–	460.9	463.3	–	–	0.007
RuZrS400	–	–	460.8	463.8	–	–	0.012
RuZrS500	–	–	460.8	463.8	161.8	1.4	0.022
RuAlS400	–	–	461.2	463.2	161.7	0.9	0.032
RuAlS500	–	–	461.0	463.2	161.9	2.0	0.037

[a] X = Si, (Si + Zr) or (Si + Al), as accordingly.
[b] Atomic ratio.

are generated when recording photoelectron spectra under a highly energetic X-ray beam impinging on the sample. This subject should also be kept in mind.

Quantitative XPS data (Table 4) show that from Ru/X atomic ratios of sulfided catalysts it can be observed that the Ru/(Si + Al) atomic ratio for samples supported on Al-SBA has the highest values what indicates a scarce dispersion of active phase, while the Ru/(Si + Zr) and Ru/Si ratios have the lowest values. These values corroborate again the same facts observed by other experimental techniques, i.e., a better dispersion of the active phase has been achieved when catalysts are supported on Si-SBA and Zr-SBA supports.

Catalysts supported on Zr-SBA, presented S/Ru values close to the stochiometric one. However, as it will be shown in the following section (H_2-TPRS), the RuZrS400 catalyst presents an excess of sulfur on the surface, H_2S or SH^- groups formed during sulfiding process [8,38], which is not forming the pyrite phase. Finally, the S/Ru ratios of RuAlS400 and RuAlS500 sulfide catalysts are higher than those of RuZrS400 and RuZrS500 ones. These catalysts, RuAlS400 and RuAlS500, present a lower dispersion of the active phase and therefore the surface sulfur will be easily detected on these catalysts.

The analysis of spent catalysts showed a decrease in the S/Ru atomic ratio, in accordance with all the experimental exposed here and the literature reports, i.e., surface sulfur elimination occur during the catalytic test.

3.2.6. H_2-TPRS

H_2-TPRS is a valuable technique which gives us information about the properties of sulfided catalysts, i.e., it can be known the different sulfur species present on a catalyst, the degree of sulfidation attained as well as the stability of the active phase [38,39]. The H_2-TPRS patterns of sulfided ruthenium catalysts are shown in Fig. 10, where H_2S removal signals are depicted. De los Reyes et al. [13] have pointed that the reduction of ruthenium sulfide based catalysts takes place in several steps. The first H_2S removal at low temperatures (T < 180 °C, peak A) is due to the surface sulfur excess which is formed during the sulfidation due to the lack of hydrogen, and/or could also be due to sulfur coordinated to surface Ru. In the second H_2S removal, between 180 and 300 °C (peak B), the elimination of surface sulfur anions occurs. Some authors have found that this band tends to disappear by sulfiding at higher temperatures, suggesting that this band arises from the reduction of an amorphous or poorly crystallize RuS_2 phase at low sulfiding temperatures [40]. Finally, at T > 300 °C (Peaks C and D) the elimination of bulk sulfur of the RuS_2-pyrite takes place leading to the metallic ruthenium phase [13,25,38,40].

Fig. 10 depicts the H_2S desorption profiles for samples sulfided at 400 °C (Fig. 10A) and samples sulfided at 500 °C (Fig. 10B). All the TPRS profiles show similar peaks in such a way that we can say that all the catalysts exhibit a general tendency in the H_2S desorption profile at both sufidation temperatures. However, if we observe the TPRS patterns obtained from catalysts sulfided at 500 °C (Fig. 10B), they slightly differ with regards to those sulfided at 400 °C (Fig. 10A). Although they both present similar H_2S desorption bands, both the relative intensities and the peak maxima positions are different depending on the sulfidation temperature employed. In this sense, when sulfiding at 500 °C the signals at T < 300 °C decreases in intensity, while those at T > 300 °C are more defined what suggests that a higher amount of pyrite-type structure is formed, in accordance with previous works [13] and XRD data analyses previously exposed. Castillo-Villalón et al. [40] have recently reported that the amount of H_2S evolving from species that are reduced at low or at high temperatures depends on the sulfidation temperature. Thus, in so far as the sulfidation temperature increases, the H_2S evolving from species reduced at high temperature does, in detriment to some species that are reduced at low temperatures. By increasing the sulfidation temperature, some ruthenium sulfided species found when sulfiding at 400 °C, are transformed into more stable RuS_2 species when sulfiding at 500 °C and that is why catalysts sulfided at 500 °C present these bands more intense. Moreover, the peak maxima shift at higher temperatures, being this fact much more important in the bands at T > 300 °C which are related to the reduction of RuS_2-pyrite phase. The formation of small particles highly dispersed as seen from TEM images probably strongly interacting with the support makes necessary a higher temperature to reduce them into the ruthenium metallic form.

In order to quantify the amount of H_2S desorbed at each temperature, the H_2S desorption curves have been decomposed as plotted in Fig. 10 that corresponds to RuSiS500 sample. In all cases the H_2S evolving profiles have been adjusted by adding four peaks: peaks A

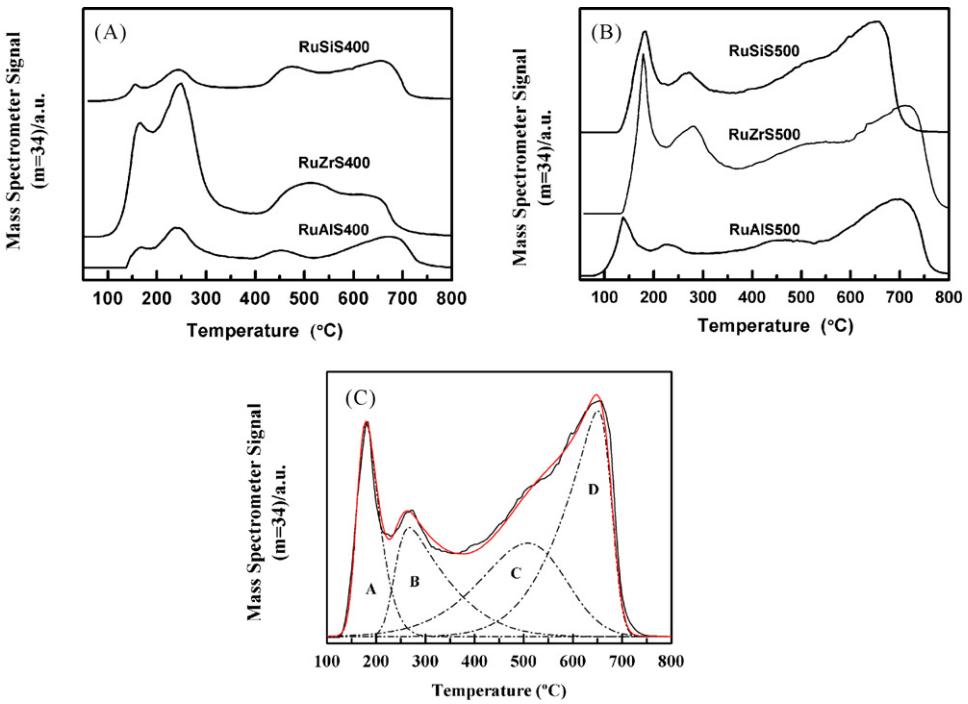

Fig. 10. Mass 34 (H_2S) signal from sulfur temperature-programmed reduction (H_2S-TPRS) of: (A) Sulfided catalysts at 400 °C, (B) Sulfided catalysts at 500 °C and (C) RuSiS500 catalyst.

and B, previously described; meanwhile peaks C and D have been considered as the process of elimination of bulk sulfur from pyrite structure leading to metallic ruthenium. A similar profile at high temperatures has been reported by other authors [40,41], i.e., the asymmetry of this band, which can be decomposed into two bands, is due to a surface reduction followed by bulk reduction [39]. The values compiled in Table 5 shows that the total amount of H_2S desorbed is lesser for catalysts sulfided at 400 °C, except the catalyst supported on Zr-SBA which present a similar amount of H_2S desorbed. The differences found on RuZrS400 and RuZrS500 lie in the temperature of desorption of H_2S. Thus, by increasing the temperature, the H_2S evolved in peak B decreases and that of peaks C and D increases. As stated before, at 400 °C there is a great proportion of amorphous or poorly crystallize RuS_2 phase, meanwhile at 500 °C the Peak B decreases considerably increasing peaks C and D, i.e., the presence of well-crystallize RuS_2-pyrite phase prevails. On the other hand, the sample supported on Si-SBA presents a sharp increase in the H_2S evolved on each peak at 500 °C of sulfiding temperature. Not only a greater formation of ruthenium sulfide in the form of pyrite but also the presence of amorphous ruthenium sulfide (peak B) and sulfur excess on the surface (Peak A), are higher. Finally, the sample prepared on Al-SBA presents an increase in the H_2S eliminated on peaks C and D at 500 °C although this increment is less pronounced than for the other two samples.

Table 5
H_2S desorbed in the different peaks of the TPRS profiles.

	Peak A	Peak B	Peak C	Peak D	Total
	$\mu mol\ H_2S\ g^{-1}$				
RuSiS400	9.0	85.0	86.1	159.6	339.8
RuSiS500	107.7	124.9	182.5	242.9	658.1
RuZrS400	103.7	386.7	186.2	145.4	822.0
RuZrS500	74.1	172.1	212.3	373.3	831.9
RuAlS400	13.8	56.3	27.3	148.1	245.5
RuAlS500	48.1	66.0	54.3	295.1	463.6

In view of the above results it can be considered that after sulfidation at 500 °C, RuSiS500 and RuZrS500 present a greater proportion of RuS_2-pyrite phase than RuAlS500 catalyst.

4. Discussion

The hydrodesulfurization of DBT over ruthenium sulfide supported on SBA type materials mainly undergoes through the direct desulfurization route (DDS) being biphenyl the main product found in all cases, i.e., the hydrogenolysis reaction is dominant over hydrogenation (Fig. 2). Catalysts supported on Si-SBA and Zr-SBA displayed higher activity than that supported on Al-SBA at all studied temperatures and at both sulfiding temperatures.

Characterization results reveal that after the sulfidation processes the formation of RuS_2 with pyrite-type structure occurs, which is the active phase in ruthenium sulfide based catalysts [8]. The role of the sulfiding temperature on the catalytic behaviour could be explained by the presence of more pyrite-type structure at 500 °C, and so all the catalysts exhibit an enhanced activity. Besides, this pyrite-type structure is maintained after the catalytic test as observed from XRD measurements. Contrary, the catalysts sulfided at 400 °C suffer a sulfur loss during the catalytic test as confirmed by XRD diffractograms, where a loss in the RuS_2 diffraction domains is observed along with the appearance of a new diffraction peak ascribed to metallic ruthenium (Fig. 5C). The decrease in the formation of hydrogenation products at $T > 300$ °C, i.e., CHB, clearly indicates that a metallic phase is present. The S/Ru atomic ratios obtained from XPS (Table 4) also show this fact, a considerable decrease in this ratio is observed. It is fully described in the literature that upon a hydrogen atmosphere, as that found during the catalytic run, some S^{2-} or S_2^{2-} may be in a first step transformed into new SH groups but some SH species may also be released as H_2S, although an excessive sulfur depletion of the surface leads to inactive sites for hydrotreating reactions; at the same time the formation of metallic Ru^0 can also take place.

Moreover, the influence of the support is directly related with the dispersion of the active phase, being a key factor on the catalytic

behaviour of these systems. In this sense, catalysts supported on Si-SBA (RuSiS400 and RuSiS500) and Zr-SBA (RuZrS400 and RuZrS500) present smaller and more dispersed RuS_2 particles than the catalysts supported on Al-SBA as it is clearly seen by XRD, TEM and XPS, turning out to be more active in the HDS of dibenzothiophene. The particles sizes hardly change during the catalytic run mainly for the catalysts sulfided at 500 °C, due to the stability of the pyrite phase formed. Regarding the selectivity values, the formation of small particles induces some preferential exposed planes, favouring the hydrogenation pathway as reported for other supported ruthenium sulfide catalysts [13–25] what reveal the sensitivity to the structure of the RuS_2. Our results are in agreement with this statement, being RuAlS400 and RuAlS500 catalysts, with the highest particles sizes, the catalysts that provide the lowest values of selectivity to CHB, product formed in the hydrogenation route.

The acidity values found for this family of catalysts are not directly related to the catalytic activity as long as RuSiS400 catalyst, with the lowest acidity, is more active than RuAlS400 with an acidity value much higher. Thus catalysts acidity is not a determining factor for the enhancement of HDS activity as reported by other authors [12–42]. It has been published in the literature that ruthenium surfaces covered by monolayers of adsorbed sulfur [43] are prone to hydrogen activation. In this regard, Lacroix et al. [44] in a study of ruthenium sulfided systems partially desulfurized, found, from ^1H NMR experiments, the existence of H^- species forming SH groups and H^+ species chemisorbed on CUS sites of Ru cations. Literature devoted to hydrotreating catalysts have come to an agreement considering that the reactants are adsorbed on CUS sites. In this regard, Berhault et al. [30] found, after sulfiding, coordinatively unsaturated Ru species having 1, 2, 3 or more sulfur vacancies that can play a double role: on one hand should activate hydrogen and on the other hand should adsorb the reactants. Therefore our sulfided catalysts should have on the surface both, SH^- and CUS sites that are involved in the ammonia chemisorption process. There is not a direct correlation between the H_2S released from H_2-TPRS experiments (Table 5) and the ammonia evolved from NH_3-TPD ones (Table 3). It should be also kept in mind those ammonia molecules directly adsorbed to the material support that explains why the RuAlS400 catalyst desorbs much more ammonia than RuSiS400 one in spite of the fact that both samples present similar H_2S profiles in the H_2-TPRS experiments, i.e., there are ammonia molecules directly interacting with Al^{3+} ions. Nonetheless there is a great difference between the H_2S and NH_3 evolved from RuZrS400 catalyst and the values obtained for RuSiS400 and RuAlS400 counterparts. Berhault et al. [29] in a study about the acidic properties of RuS_2/SiO_2 catalyst determined by infrared spectroscopy of adsorbed pyridine, suggested that ruthenium cations presenting low sulfur coordination are not involved in the pyridine chemisorption process. The same fact could be happening here as long as catalysts supported on Si-SBA (RuSiS400) and Al-SBA (RuAlS400), supports much less acidic than Zr-SBA one, should present ruthenium cations with lower sulfur coordination (these two catalysts liberate much less H_2S in the H_2-TPRS experiment), that do not participate in the ammonia chemisorption. The presence of zirconium in the mesoporous structure should have the role of stabilizing the RuS bond strength avoiding its overrreduction when the catalyst is placed under HDS conditions and is responsible of the lower presence of ruthenium cations with low sulfur coordination that do not chemisorb ammonia.

The catalytic results reported here are similar than those reported for alumina supported ruthenium sulfide–cesium catalysts with metal loadings between 4 and 12 wt% [45]. The strong interaction of RuS_2 particles with the pores leads to an equivalent performance to that obtained when alumina is doped with Cs^+ ions [17].

The most striking results exposed here come from the influence of the support on the catalytic activity data. Catalysts supported on Si-SBA and Zr-SBA posses a similar activity pattern. Recently, Eliche-Quesada et al. [18] prepared a family of catalysts supported on MCM-41 and ZrMCM-41 type materials and obtained a sharp increase in the activity with the catalysts supported on ZrMCM-41, i.e., the incorporation of zirconium into the framework structure turned out to be very important to improve the dispersion of the active phase and to stabilize the Ru-S bond of the pyrite-like structure, having the same role that the incorporation of Cs to the catalysts [17,45]. Comparing our DBT conversion values with those obtained for ruthenium sulfided catalysts supported on MCM-41 type materials with a 7 wt% of ruthenium and tested in similar experimental conditions, it is observed that the catalyst supported on pure mesoporous silica MCM-41 possesses a much lower activity than our catalysts supported on Si-SBA (RuSi400 and RuSi500), that possess high activities (Fig. 1). While, that supported on ZrMCM-41 only presents a similar conversion than our catalyst supported on Zr-SBA (RuZrS500) at 320 °C, at higher temperatures (360 °C) our catalyst reaches a value close to 100%. The different behaviour could be due to the dispersion achieved in both support is distinct, whereas on Zr-SBA all the ruthenium sulphide particles are located in the pores, on the ZrMCM-41 an important fraction is on the external surface where is less stable and can be reduced during the experimental conditions. Moreover, the stability with time on stream revealed the higher stability of our catalyst (RuZrS500), which maintained a conversion close to 100% after nine hours working, while the catalyst supported on ZrMCM-41 [18] decreased its conversion after 8 h on stream. Moreover, Eliche-Quesada et al. [18] also prepared a ruthenium sulfided catalyst supported on a commercial support such as γ-Al_2O_3, being this catalyst less active than that supported on ZrMCM-41 and therefore less active than our catalysts supported on SBA type materials.

The results reported here, highlight the important role that the material support plays on the stability of the active phase, i.e., SBA type mesoporous materials provide ruthenium sulfide catalysts which are more stable in the HDS reaction of DBT than MCM-41 mesoporous one, what could be related to the higher diameter of pores which leads to a better filling of them with the ruthenium sulphide.

5. Conclusions

Ruthenium sulfided catalysts supported on SBA type materials turned out to be highly active in the HDS of DBT reaction. The formation of the ruthenium sulfide with pyrite-like structure was achieved at both sulfiding temperatures studied here, although at 500 °C a greater formation of such a compound occurs which is also more stable. Pure mesoporous silica (Si-SBA) and that doped with zirconium (Zr-SBA) were the best supports for this family of catalysts as long as a higher dispersion of the active phase into the mesoporous channels is achieved with a high stability of the RuS_2 particles due to a stronger interaction with the support. However, the support Al-SBA provided catalysts with a poor dispersion of the active phase and therefore less active in the HDS reaction.

Acknowledgements

We gratefully acknowledge the support from the Ministry of Science and Innovation, Spain (Ministerio de Ciencia e Innovación, España) through the project MAT2009-10481 and FEDER funds. A.R.P. thanks to CONACyT (México) for its financial support (Scholarship No. 189933). A.I.M. also thanks the Ministry of Science and Innovation, Spain (Ministerio de Ciencia e Innovación, España) for a Juan de la Cierva contract.

References

[1] http://www.dieselnet.com/standards/eu/ld.php.
[2] C.S. Hsu, P.R. Robinson, Practical Advances in Petroleum Processing, vol. 1, Springer, USA, 2006, pp. 49–58.
[3] M. Egorova, R. Prins, J. Catal. 224 (2004) 278–287.
[4] C. Song, X. Ma, Appl. Catal. B: Environ. 41 (2003) 207–238.
[5] M. Gómez-Cazalilla, A. Infantes-Molina, R. Moreno-Tost, P.J. Maireles-Torres, J. Mérida-Robles, E. Rodríguez-Castellón, A. Jiménez-López, Catal. Today 143 (2009) 137–144.
[6] W. Qian, T. Kawano, A. Funato, A. Ishihara, T. Kabe, Phys. Chem. Chem. Phys. 3 (2001) 261–266.
[7] T.A. Pecoraro, R.R. Chianelli, J. Catal. 67 (1987) 430–445.
[8] J.A. De Los Reyes, S. Göbölös, M. Vrinat, M. Breysse, Catal. Lett. 5 (1990) 17–24.
[9] S.J. Liaw, R. Lin, A. Raje, B.H. Davis, Appl. Catal. A 151 (1997) 423–435.
[10] J.A. De Los, Reyes, Appl. Catal. A 322 (2007) 106–112.
[11] J. Quartararo, S. Mignard, S. Kasztelan, J. Catal. 192 (2000) 307–315.
[12] B. Pawelec, R.M. Navarro, P. Castao, M.C. Álvarez-Galván, J.L.G. Fierro, Energy & Fuels 23 (2009) 1364–1372.
[13] J.A. De Los Reyes, M. Vrinat, C. Geantet, M. Breysse, Catal. Today 10 (1991) 645–664.
[14] G.M. Dhar, B.N. Srinivas, M.S. Rana, M. Kumar, S.K. Maity, Catal. Today 86 (2003) 45–60.
[15] M. Breysse, P. Afanasiev, C. Geantet, M. Vrinat, Catal. Today 86 (2003) 5–16.
[16] R.R. Chianelli, M. Daage, M.J. Ledoux, Adv. Catal. 40 (1994) 177–232.
[17] A. Ishihara, J. Lee, F. Dumeignil, M. Yamaguchi, S. Hirao, E.W. Qian, T. Kabe, J. Catal. 224 (2004) 243–251.
[18] D. Eliche-Quesada, E. Rodríguez-Castellón, A. Jiménez-López, Micropor. Mesopor. Mater. 99 (2007) 268–278.
[19] L. Vradman, M.V. Landau, M. Herskowitz, V. Ezersky, M. Talianker, S. Nikitenko, Y. Koltypin, A. Gedanken, J. Catal. 213 (2003) 163–175.
[20] G.M. Dhar, G.M. Kumaran, M. Kumar, K.S. Rawat, L.D. Sharma, B.D. Raju, K.S. RamaRao, Catal. Today 99 (2005) 309–314.
[21] J.M. Kim, G.D. Stucky, Chem. Commun. 13 (2000) 1159–1160.
[22] K. Szczodrowski, B. Prélot, S. Lantenois, J. Zajac, M. Lindheimer, D. Jones, A. Julbe, A. van der Lee, Micropor. Mesopor. Mater. 110 (2008) 111–118.
[23] M. Gómez-Cazalilla, J.M. Mérida-Robles, A. Gurbani, E. Rodríguez Castellón, A. Jiménez-López, J. Solid State Chem. 180 (2007) 1130–1140.
[24] S. Brunauer, P.H. Emmet, E. Teller, J. Am. Chem. Soc. 60 (1938) 309–319.
[25] C. Dumonteil, M. Lacroix, C. Geantet, H. Jobic, M. Breysse, J. Catal. 187 (1999) 464–473.
[26] M. Lacroix, C. Midoratos, M. Breysse, T. Decamp, S. Yuan, in: F. Solymosi, P. Tétànyi, L. Guezi (Eds.), New Frontiers in Catalysis, Elsevier, Budapest, 1993, p. 597.
[27] B. Chandret, S. Sabo-Etienne, in: R.B. King (Ed.), Encyclopedia of Inorganic Chemistry, vol. 7, Wiley, Chichester, 1994.
[28] T.L. Stuchinskaya, M. Musawir, E.F. Kozhevnikova, I.V. Kozhevnikov, J. Catal. 231 (2005) 41–47.
[29] G. Berhault, M. Lacroix, M. Breysse, F. Maugé, J.C. Lavalley, H. Nie, L. Qu, J. Catal. 178 (1998) 555–565.
[30] G. Berhault, M. Lacroix, M. Breysse, F. Maugé, J.C. Lavalley, L. Qu, J. Catal. 170 (1997) 37–45.
[31] V. Mazzieri, F. Coloma-Pascual, A. Arcoya, P.C. L'Argentière, N.S. Fígoli, Appl. Surf. Sci. 210 (2003) 222–230.
[32] F.A. Cotton, G. Wilkinson, C.A. Murillo, M. Bochman, Advanced Inorganic Chemistry, John Wiley and Sons. Inc, USA, 1999, pp. 1012–1013.
[33] S.E. Livingstone, in: J.C. Bailar, M.J. Emeléus, R. Nyholm, A.F. Trotman-Dickenson (Eds.), Comprehensive Inorganic Chemistry, vol. 3, Pergamon Press, Oxford, 1973, pp. 1191–1193.
[34] J.F. Moulder, W.F. Stickle, P.E. Sobol, K.D. Bomben, in: Jill Chastain (Ed.), Handbook of X-ray Photoelectron Spectroscopy, Perkin-Elmer, Minnesota, 1992.
[35] P.C.H. Mitchell, C.E. Scott, J.P. Bonnelle, J.G. Grimblot, J. Catal. 107 (1987) 482–489.
[36] P. Reyes, M.E. König, G. Pecchi, I. Concha, M. López Granados, J.L.G. Fierro, Catal. Lett. 46 (1997) 71–75.
[37] R. Navarro, B. Pawelec, J.L.G. Fierro, P.T. Vasudevan, Appl. Catal. A 148 (1996) 23–40.
[38] P.J. Mangnus, A. Riezebos, A.D. Vanlangeveld, J.A. Moulijn, J. Catal. 151 (1995) 178–191.
[39] F. Labruyère, M. Lacroix, D. Schweich, M. Breysse, J. Catal. 167 (1997) 464–469.
[40] P. Castillo-Villalón, J. Ramírez, F. Maugé, J. Catal. 260 (2008) 65–74.
[41] M. Wojciechowska, M. Pietrowski, B. Czajka, Catal. Today 65 (2001) 349–353.
[42] C. Sun, M.J. Peltre, M. Briend, J. Blanchard, K. Fajerwerg, J.M. Krafft, M. Breysse, M. Cattenot, M. Lacroix, Appl. Catal. A 245 (2003) 245–256.
[43] Y.J. Kuo, R.A. Cocco, B.J. Tatarchuk, J. Catal. 112 (1988) 250–266.
[44] M. Lacroix, S. Yuan, M. Breysse, J. Catal. 138 (1992) 409–412.
[45] A. Ishihara, H. Godo, R. Kanamori, W. Qian, T. Kabe, Appl. Catal. A 182 (1999) 345–355.